Accepted in the Journal of "Infrared Physics & Technology" in Jan 2023

Research on development of aspheric diffractive optical element for mid-infrared imaging

Neha Khatri[a,b*], Sonam Berwal[a,b], K Manjunath[a,b], Bharpoor Singh[a],Vinod Mishra[b,c]and Saurav Goel[d,e]

[a] Department of Manufacturing Science & Instrumentation, CSIR-CSIO, Sector 30-Chandigarh, India 160030
[b] Academy of Scientific & Innovative Research (AcSIR), CSIR-CSIO, Sector 30-Chandigarh, India 160030
[c] Mechanical Design and Fabrication Facility, CSIR-CSIO, Sector 30-Chandigarh, India 160030
[d] School of Engineering, London South Bank University, 103 Borough Road, London SE1 0AA, UK
[e] Department of Mechanical Engineering, University of Petroleum and Energy Studies, Dehradun, 248007, India

*Corresponding author: nehakhatri@csio.res.in

Abstract:

The aspheric diffractive lens reduces chromatic aberration in precision infrared optical systems. With the advancement in micro-optics, conventional lenses are replaced by aspheric, diffractive and hybrid surfaces to fulfil the requirements of miniaturized design of optical devices. This paper covers the detailed aspects of hybrid aspheric diffractive optics from design to manufacturing by precision machining. The germanium aspheric diffractive lens is designed using Zemax OpticsStudio® for Medium Wave Infrared (MWIR) range to achieve an aberration-free and diffraction-limited surface. The designed surface is fabricated by the diamond turning process. The developed surface is characterized by profile and diffractive structure quality. The results demonstrate the fabricated lens with a diffractive structure step height error of 0.001 µm and radial position error of 1 µm. A high-quality aspheric diffractive lens is fabricated with 99.57% diffraction efficiency.

Keywords: Brittle machining, Diamond turning, Aspheric diffractive optical element, Roughness, Optical design

1. Introduction

With the evolution of Infrared (IR) technology, there is a growing demand for high-performance optical systems, especially in defence, modern military reconnaissance, astronomy, and aerospace applications. Rapid target detection and real-time tracking with accurate target measurement have become the spotlight in the development of optical systems. For such critical applications, the refractive lenses and traditional optics are being replaced by Diffractive Optical Elements (DOEs) with sub-structures on the aspheric profile to fulfil the requirements of lightweight and compact optical devices [1]. It is known that refractive optical elements with the spherical profile are not suitable for observations due to the large chromatic and spherical aberration caused by the dispersion of light from optical components [2]. Furthermore, these optical losses also occur due to the material properties and profile of the element. In addition, conventional optics is also unsuitable for astronomical instruments and IR applications because several optical elements are often required to achieve the desired performance, which makes the overall system bulky. The DOEs have the capability to improve the performance of optical systems by reducing chromatic aberration and size. Besides the advancement of optical components with size and profile, surface integrity can also enhance the functionality of the optical systems in many ways, such as the performance of the

device, diffraction efficiency, optical aberrations, and reliability of the systems. These optical components require ultra-precision fabrication methods with optimum outcomes to achieve excellent surface quality.

There are various fabrication techniques of diffractive optical elements such as lithography [3, 4], replication method using moulding, embossing [5-7], direct machining using ion beam technique and diamond turning [8-13] etc. Each method has its benefits and drawbacks. However, Single Point Diamond Turning (SPDT) is the most appropriate technique for the fabrication of DOEs with flat and spherical/aspheric surfaces for visible and infrared wavelength. Fig. 1 shows the schematic of SPDT machining of hybrid (curved surface with diffractive structures). SPDT is widely used to fabricate highly accurate mirrors, varifocal lenses, infrared optics and various applications in a different light spectrum range. Aluminium, glass, PMMA, and nickel-silver alloy are widely used as material for visible range [14-16]. Whereas silicon (Si), zinc sulphide (ZnS), zinc selenide (ZnSe) and germanium (Ge) are employed for IR optics [17, 18].

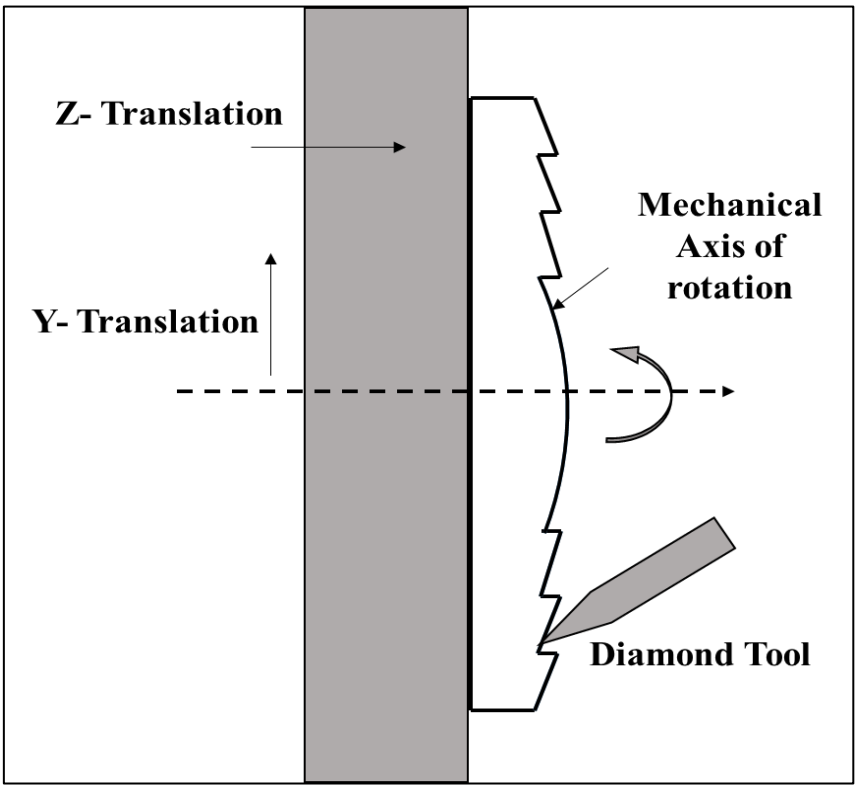

Fig. 1. Single-point diamond turning of a diffractive lens.

For Mid Wave Infrared (MWIR), i.e., for 3-8μm wavelength, single-crystal germanium is an appropriate optical material due to its high permeability, good thermal sensitivity, and high refractive index [19]. Germanium is often treated as difficult-to-machine material due to its brittleness, tool wear and chemical reactivity with the tool. The

challenges in the machining of germanium for various applications have been investigated by many researchers in the past decade. Blake and Scattergood have described the ductile mode machining of germanium. The compressive stresses on the surface during machining is obtained by using the negative rake tool [20]. Due to increased cutting forces, fabricating diffractive optical elements on brittle materials increases the tool wear rate. This results in deterioration of the surface quality of the optical component [21, 22]. The other challenges in fabrication aspects, such as the effects of machining parameters on surface integrity and profile accuracy, are also discussed [15, 19, 21]. Some researchers have used ion beam milling operation to fabricate the Fresnel lenses on different materials like aluminium alloys, and BK_7 glasses used in visible range [12, 23]. Where, aspheric lenses on Ge, Si , ZnSe and ZnS etc. applicable in infrared optics have been fabricated using diamond turning with less than 0.3 μm profile error and 5nm surface roughness [9]. One of the vital characteristics associated with ductile mode cutting is the nature of the chip formation. Significant work has been reported on the chip formation mechanism. Jasinevicius et al. demonstrated the machined surface quality based on chip removal during the machining of Ge [24].

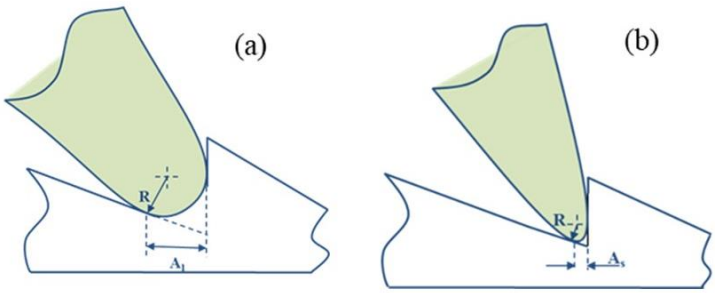

Fig. 2. Shadowing effect comparison of (a) large radius tool and (b) small radius tool.

The specification of the cutting tool plays a significant role in determining the surface quality. For the fabrication of DOEs, the appropraite tool nose radius selection is essential. As, tool nose radius seriously influences the surface quality and also affects the shape and size of sub-structures and the diffraction efficiency and performance [25]. Fig. 2 (a) and (b) shows the shadowing effect of large and small radius tools. The larger nose radius tool has a significant shadowing effect, covering a large area and cutting less material, whereas its contrast in a small radius tool with a sharp tip. Thus, a small or half radius tool for the fabrication of DOEs is more suitable for generating sharp edges steps on the surface.

The wavefront emerging from the non-uniform blazed structure due to shadowing has some discontinuities which affect the diffraction efficiency. When a beam of light incident from below passes through the diffractive structure, it is redirected, and the beam emerging from each period of grating Λ becomes a beamlet of width $\Lambda`$ as shown in Fig. 3. The significant shadowing effect causes the step height error, significantly decreasing the diffraction efficiency. The Diffraction efficiency for continuous relief profile of diffractive is depicted by Eq. 1.1.

$$\eta = \left(\frac{sin(\pi\beta)}{\pi\beta}\right)^2 \tag{1.1}$$

where, $\beta=((\lambda_0-\lambda))/\lambda$, here λ is the designed wavelength, λ_0 is the wavelength achieved after fabrication i.e. working wavelength that is calculated with the help of $\lambda_0=(N-1)d_0$, where d_0 is the step height that is fabricated and N is the refractive index of the material.

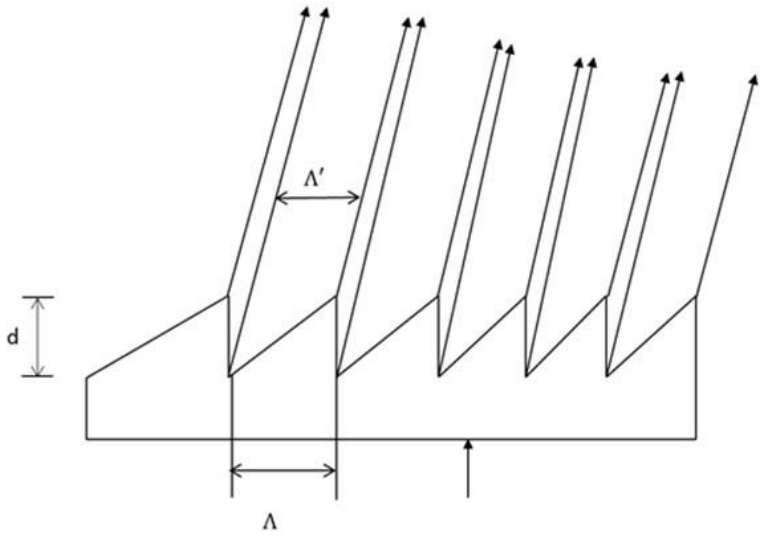

Fig. 3. Wavefront discontinuities due to step height error caused by shadowing effect.

The diffraction efficiency decreases quickly when the working wavelength deviates far from the design wavelengths, which deteriorates the imaging quality. The conventional optical components cannot satisfy the requirements of the advanced optical instruments for IR range [18]. The DOEs with an aspheric profile can improve chromatic and spherical aberrations and enhance the quality of the optical system. This paper aims to develop an approach for ultra-precision machining the aspheric diffractive lens with reduced error and high diffraction efficiency. The experiments are carried out to develop a Ge aspheric DOE by SPDT. The profile error compensation is done to achieve better profile accuracies. The key optical design, fabrication, and metrology aspects for developing germanium aspheric diffractive optical elements are investigated and discussed in detail.

2. Optical Design

An optical system is associated with numerous aberrations, including monochromatic (spherical aberration, defocus, coma, astigmatism, field curvature, image distortion) and chromatic (longitudinal and transverse). However, almost all imaging systems suffer from chromatic aberrations, in which the light of different wavelengths creates focal spots at different spatial locations. This phenomenon declines the performance of both imaging and non-imaging

systems under broadband illumination [26]. Hence an optical system without chromatic-aberration correction will form the defocused images.

Greisukh et al. [27] presented a technique to selecting the layout of the optical scheme for ultra-high-aperture dual-range athermal infrared objectives. Provided a choice of optical materials like IRG22, Ge, ZnS, IRG22, IRG24 and correction of optical aberrations. Also, presented effective focal length f^{l} = 40 mm that is within the half-field angle ≤ 9.75° form an image at the Nyquist frequency of the microbolometer (NN = 30 mm^{-1}) with a contrast T ≥ 0.5. Also, there are attempts made by multilayer diffractive optical elements and highlighted the benefit of adding a high index gap material to reduce the Total internal reflection (TIR) and enhance the optical performance [28, 29].

In this study, different approaches are employed to minimize the spherical and chromatic aberration. An optical design software (Zemax OpticStudio®, version 22.1) is utilized to simulate the different lens systems. Initially, the design of an optical system starts with the combination of different spherical (concave and convex) lenses. However, with the four optical elements, the aberrations still affect the whole field of the system. Also, the proposed technique of four lens system is cumbersome since the number of elements are more. The alignment of lenses also makes the system more complex, expensive and bulky.

An alternative to minimize the spherical aberrations is to use an aspherical lens by replacing the two spherical lenses. Fig. 4 illustrates the layout of first-lens system that contains two conventional lenses (L1, L2) and an aspheric lens (L3). The aspheric surface is used in various applications to eliminate spherical aberration; such defined by the conic constant (K) having multiple values according to the surface type, i.e. hyperbolic, parabolic, elliptical, and spherical. The aspheric surface is represented by Eq. 2.1 [30].

$$\boldsymbol{Z_a = \frac{Rx^2}{1+\sqrt{1-(1+k)c^2x^2}} + Ax^4 + Bx^6 + Cx^8} \qquad (2.1)$$

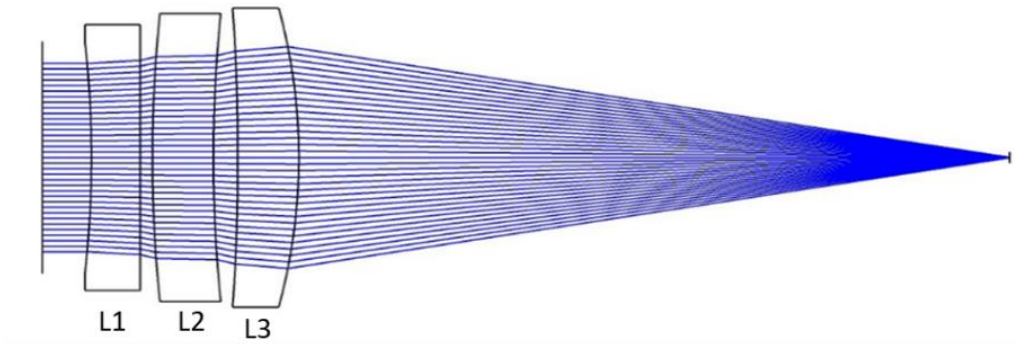

Fig. 4. Layout of first-lens system.

However, the other aberrations, like chromatic aberration, could not be compensated by the aspheric surface. Hence, an aspheric diffractive lens is designed and fabricated to eliminate the both spherical and chromatic aberration for better image quality. An even aspherical surface with diffractive properties is defined in Zemax by the Binary 2 element. A diffractive lens comprises multiple zones that transmit a phase change across the optical surface. The diffractive profile has its equation which depends on the wavelength of light for which it is designed, step height, the material's refractive index, and diffractive constants. The combined profile of the aspheric and diffractive is represented by Eq. 2.2 and Eq. 2.3.

$$\boldsymbol{Z_d = \frac{(Ax^2+Bx^4+Cx^6+Dx^8\ldots)}{N-1} - [dmax * Int\frac{|(c1x^2+c2x^4+c3x^6+c4x^8\ldots)|}{\lambda}]} \tag{2.2}$$

$$\textbf{Total sag height (Z) } = Z_a + Z_d \tag{2.3}$$

where, Z is total sag height, Z_a = sag height of aspheric profile, Z_d= sag height of diffractive profile, K = conic constant, R = radius of curvature, x = radial distance from center to the periphery, λ= wavelength of light, N = refractive index of the material, A, B, C…. = aspheric constants, C1, C2, C3, C4…. = diffractive constants, and d_{max}= step height of the diffractive groove.

In the meantime, the aspheric coefficient of the diffractive optical element can be utilized to balance the higher-order aberrations. The Binary 2 surface type introduces continuous phase change across the surface according to the following polynomial expansion as shown in Eq. 2.4.

$$\boldsymbol{\varphi = M\sum_{i=1}^{N} A_i \rho^{2i}} \tag{2.4}$$

where N is the number of polynomial coefficients in the series, Ai is the coefficient on the $2i^{th}$ power of ρ, which is the normalized radial aperture coordinate, and M is the diffraction order. Table 1 shows the detailed data and configuration of polynomial coefficients for the aspheric diffractive lens.

Table 1

Design specifications for aspheric diffractive lens.

Material	**Germanium**
Diameter (D)	20 mm
Wavelength (λ)	4.2 µm
Refractive Index (n)	4.003

Centre thickness (CT)	4 mm
Radius of front surface (R1)	104.745mm
Radius of rear surface (R2)	Nearly flat
Diffraction order (M)	1
Aspheric constants A, B, C, D	-0.2177E-06, -0.1679E-08, -0.4868E-10, 0.1152E-11
Diffractive constants C1, C2, C3	-0.4178E-03, 0.2402E-06, -0.5121E-08
Step height (d)	1.388 µm

The system is optimized using the multiparameter optimization method to achieve aberration-free and diffraction limited surface. The various parameters like the Strehl ratio, airy radius, and RMS radius are compared at different wavelengths in the MWIR range (3-8 µm) to improve image quality. It is concluded that the highest value of the Strehl ratio (0.92) is obtained at 4.2 µm wavelength, indicating less deviation in the optical surface from its nominal form. The depth of the grating features for the designed wavelength is calculated by Eq. 2.5.

$$d = \frac{\lambda}{(n_{DOE} - 1)} \tag{2.5}$$

To enhance the system's image quality, a second-lens system is designed that employs an aspherical diffractive lens (L1) with the plano-convex lens (L2), as shown in Fig. 5. The proposed Binary 2 surface (aspherical diffractive lens) is divergent in nature; hence, a plano-convex lens is utilized to focus the incident beams at the focal point without dispersion. However, due to the presence of a conventional lens, spherical aberration is generated in the system.

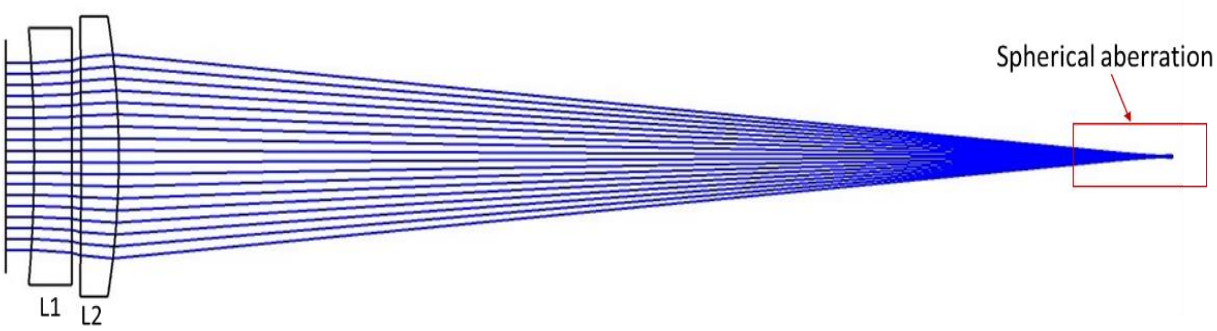

Fig. 5. Layout of second-lens system.

Further, to reduce the spherical aberration, a Binary 2 surface is employed with an aspherical lens at the wavelength (λ) of 4.2 μm to work in the IR range that can be utilized to develop miniaturized infrared cameras to provide small payload systems with thermal vision capability for both military and civilian applications. The design specifications of the aspheric convex lens are listed in Table 2.

Table 2

Design parameters for aspheric converging lens.

Material	**Germanium**
Diameter (D)	24 mm
Wavelength (λ)	4.2 μm
Refractive Index (n)	4.003
Centre thickness (CT)	5 mm
Radius of front surface (R1)	Nearly flat
Radius of rear surface (R2)	67.360 mm
Conic constant	-2.1
Aspheric constants A, B, C, D	2.236E-04, 5.256E-07, -3.325E-09, 6.322E-14

Fig. 6 shows the layout of the third-lens system that utilized the aspherical diffractive lens (L1) and the converging aspheric lens (L2). The first surface (S1) of the lens (L1) is a Binary 2 surface, which shows the properties of both aspheric and diffractive surfaces. The second surface (S2) is a planer surface.

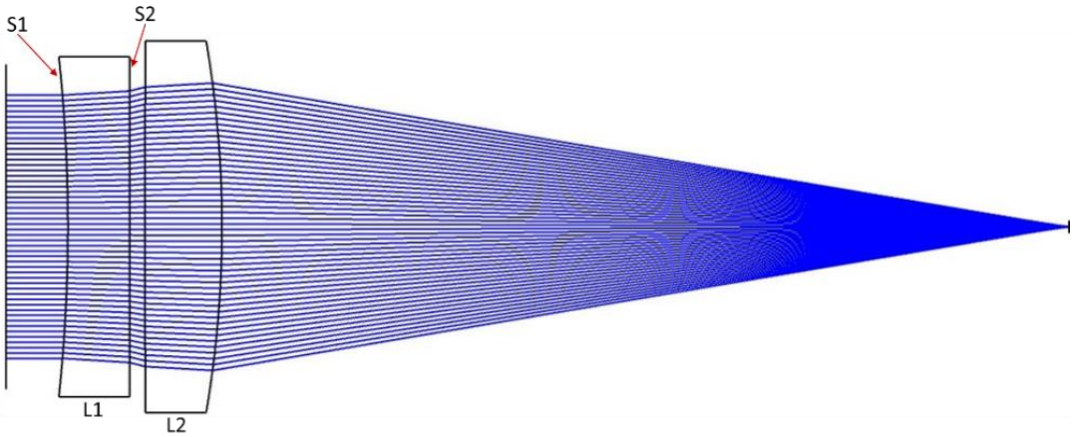

Fig. 6. Layout of third-lens system.

After designing different system configurations, the comparison of all three (first-lens, second-lens, third-lens) systems based on optical performance is carried out. As shown in Fig. 7 (a), the longitudinal aberration of the first lens system is less than 1.2 mm, Fig. 7 (b) shows the longitudinal aberration of the second system, which is less than 0.7 mm, and Fig. 7 (c) shows the longitudinal aberration of the third system, which is almost negligible**.**

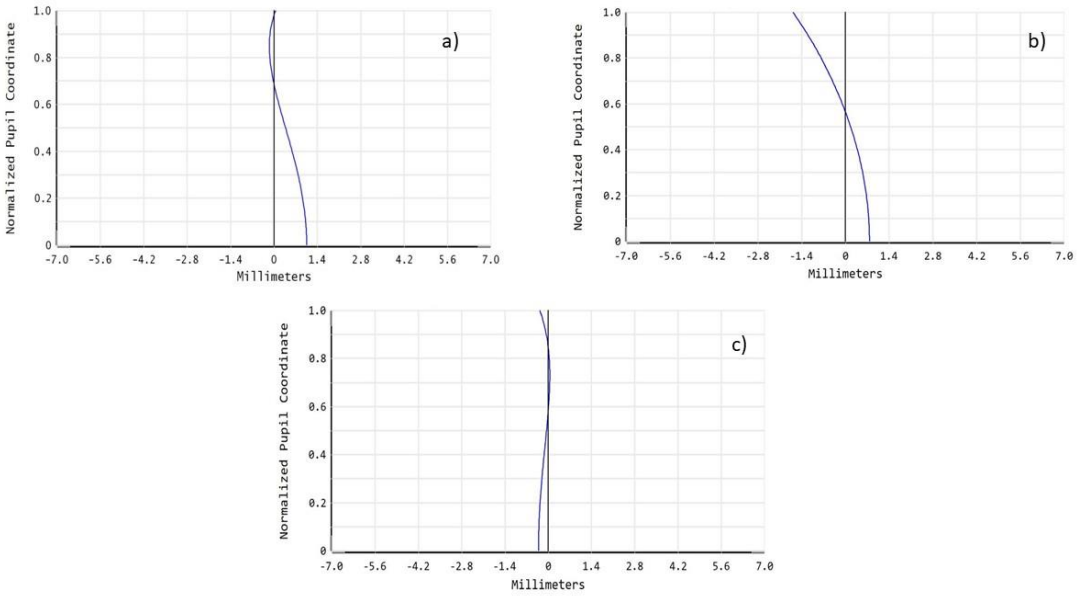

Fig. 7. Longitudinal aberration of the proposed (a) first-lens system, (b) second-lens system, and (c) third-lens system.

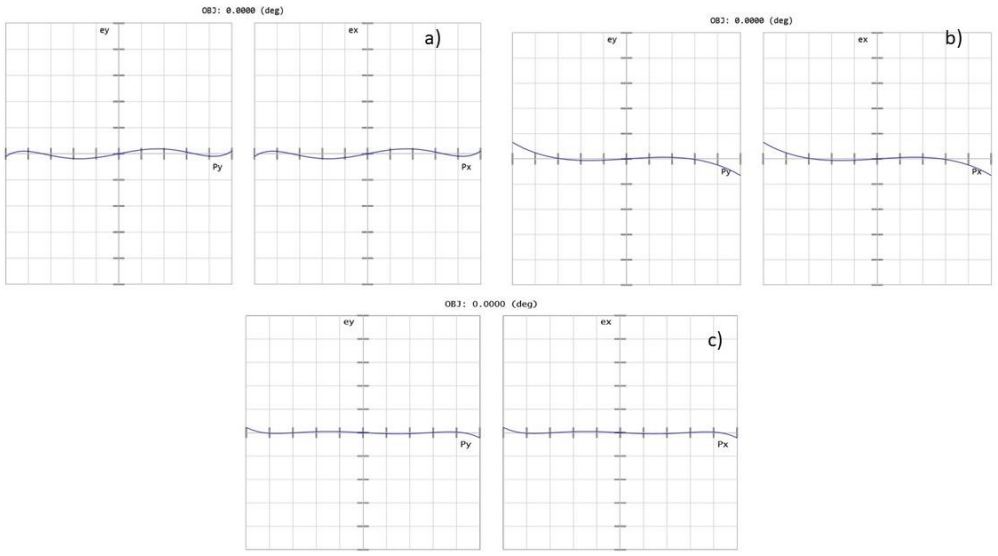

Fig. 8. Wave aberrations of the proposed (a) first-lens system, (b) second-lens system, and (c) third-lens system.

The wave aberrations of the first, second, and third lens systems are shown in Fig. 8. It can be observed that the axial chromatic aberration is much better balanced in the third-lens system (as shown in Fig. 8 (c)) than that in the

first and second lens system. Moreover, the spherical aberrations, chromatic aberrations, and coma are corrected, preferable in the third system than in the first and second systems. Fig. 9 illustrates the Modulation Transfer Function (MTF) curves of all proposed lens systems. It can be seen from Fig. 9 (c) that the MTF curve of the third-lens system is almost coincident and are very close to the diffraction-limited ideal curve. Hence, it provides better resolution and image quality than other systems.

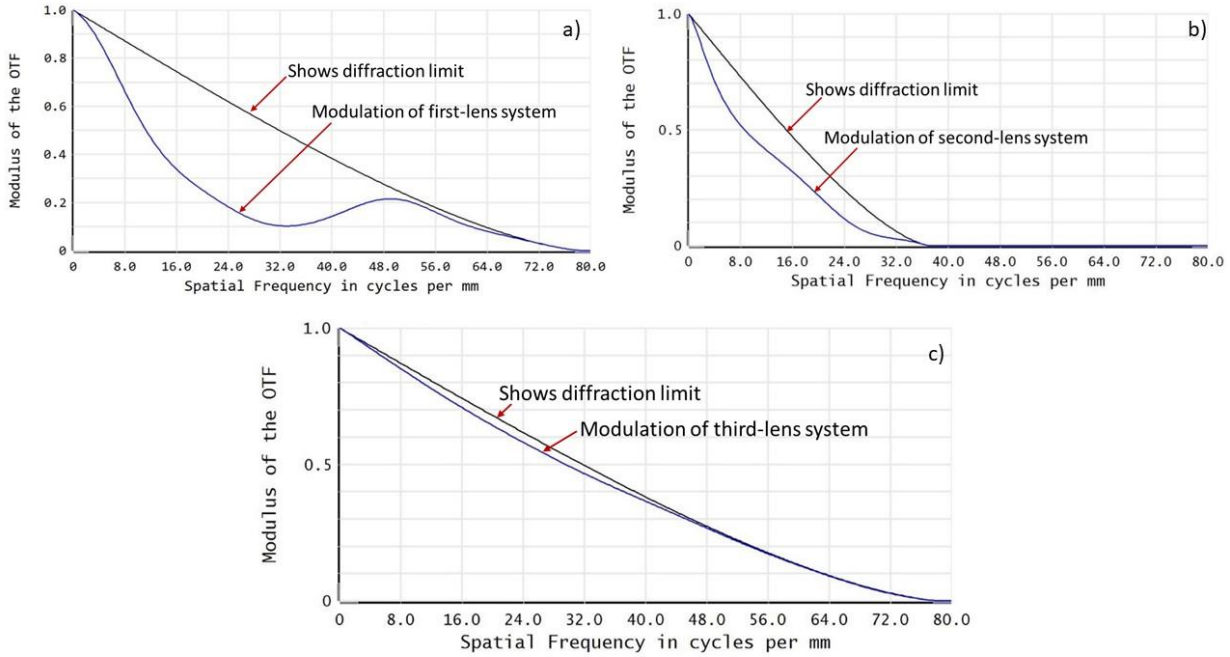

Fig. 9. MTF curve for the proposed (a) first-lens system, (b) second-lens system, and (c) third-lens system.

Based on the performance of all three lens systems, it is concluded that an aspheric diffractive lens with a converging aspheric lens is the best lens system for imaging applications. The manufacturing of conventional spherical and aspheric optical elements is straight forward and a lot of research has already been reported for the same. However, the manufacturing of hybrid aspheric and diffractive surfaces is still challenging. Hence, in current work the fabrication of the aspheric diffractive lens is taken into consideration.

3. Aspheric Diffractive Lens Fabrication

SPDT is a precision machining technique that can produce any complex shape more deterministically. SPDT process is very dynamic and sensitive toward minute changes that occur during machining, and infinitesimal change manifests immediately on the surface quality [31]. Thus, the selection of appropriate machining parameters becomes very critical, any process anomalies cause several cascading faults and affect the optical performance of the fabricated component. Bittner [32] studied the tolerance of the single point turned diffractive optical element and simulated their influence on aberrations in optical system. Gao et al. [33] proposed methods for manufacturing harmonic diffractive optical elements on soft-brittle material, Barium Fluoride (BaF_2). The optimal half-round tool

position is found out to be an effective way by eliminating the shadowing effect and scattering effect. In the case of difficult-to-cut materials due to high hardness and low machinability, factors such as sub-surface damage [19] and tool wear [22] also worsen surface quality. However, earlier research demonstrated that brittle materials could be machined in a ductile regime zone [13] with optimized cutting parameters. Rohit et al. studied the effect of machining parameters on diamond turning of germanium, and explored ductile-regime machining to explain the sub-surface damage with varying input parameters [34]. Also, earlier work by Shivani et al. proposed parameter optimization for fabrication of IR aspheric diffractive optical element using response surface methodology [35]. Thus, in this paper selection of machining parameters such as spindle speed, feed rate, depth of cut and tool overhang are made as suggested in our previous work [36].

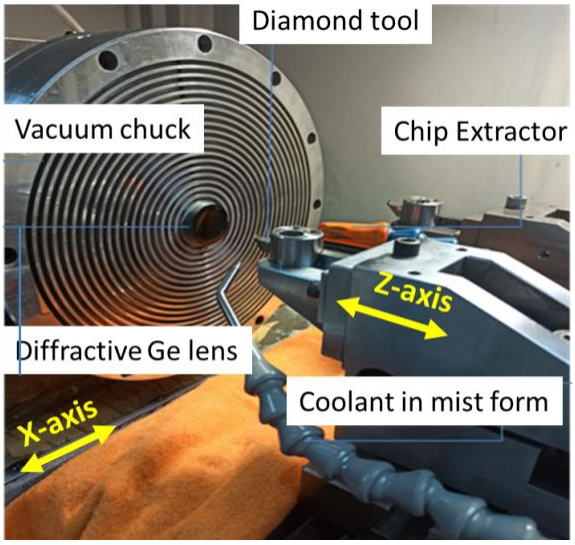

Fig. 10. Diamond Turning Machine (Nanoform 200).

Table 3

Cutting Parameters with their respective range & optimized value

Sr. No.	Cutting Parameters	Range	Optimized Value
1.	**Spindle Speed(rpm)**	1000-2000	2000
2.	**Tool Feed Rate (µm/rev)**	1-6	1
3.	**Depth of Cut(µm)**	0.5-1.5	1.5
4.	**Tool Overhang(mm)**	14-20	14

The fabrication experiments are performed on CNC ultra-precision lathe (Precitech® make Nanoform 200). Fig. 10 shows the configuration used for fabrication of the diffractive optical elements. A single crystal diamond tool with nose radius of 0.2 mm and negative rake angle (Contour Fine Tooling make) is used to achieve the desired surface quality in terms of surface form, finish and diffractive substructures dimensions. The Ge wafer of 20mm diameter is used for experimentation. The optimum value of these machining variables is represented in Table 3, which is used for the fabrication of aspheric diffractive optics.

From the design data, the step height of the diffractive grooves to be fabricated is 1.388 µm calculated from [$d_{max}=\lambda/(N-1)$]. Step height plays an important role in deciding the direction and phase of the incident light falling on the surface, which influences the efficiency of the component. The total no of diffractive zones (rings) is eight(8) with a clear aperture of 18.2 mm. The sag value for the designed aspheric diffractive surface is 0.4 mm, which is needed to calculate the number of rough cuts required to achieve the basic shape.

A tool path is designed through DiffSys (CAM software used for ultraprecision machining) software for the desired aspheric diffractive surface. This software follows a constant-angle strategy based on interpolation tolerance between the radius of curvature and tool nose radius. Using the designed values i.e., the radius of curvature (104.745mm), conic constant (K=0), and all constants (aspheric and diffractive profile), a tool path file is generated in terms of X & Z coordinates in Diffsys®, keeping the X axis increment value 1 µm. These data points (X and Z) with prologue and epilogue info (G&M codes) are then uploaded to the SPDT controller as a program file. For initial shape generation, during rough cuts, the depth of cut is 15 µm, feed rate 3 µm/rev and spindle speed 2000 rpm is considered. For fine cutting, optimized parameters are used, as mentioned in Table 3.

4. Results & Discussions

The performance and efficiency of the optical elements depend on the surface finish and profile accuracy. The measurement of Aspheric profile is quite challenging as the aspheric profile of lens is at a nanometric level. Yadav et al. [37] fabricated aspheric germanium lens and the parameters such as ROC, slope error, tilt and sag using a contact type and non-contact type interferometers. It was observed that increase in ROC beyond 13.839 mm and lens thickness over 5.10 mm will increase the spherical aberration. Thus, in the work the contact type profiler (Talysurf PGI®) and optical profiler (Coherence Correlation Interferometer (CCI)), are utilized for the profile and structures measurement of aspheric diffractive surface. After the first machining iteration surface is measured by taking a 2D scan through a contact profiler, this raw profile is then compared with the design profile (i.e., base profile, zone position and zone height extraction) through for aspheric diffractive analysis software. Fig. 11 (a) depicts the base radius of curvature of the aspheric profile, measured as 104.985 mm, deviating by 0.24mm from the design radius. The noticed profile error (Pt) is 0.9669 µm after the first cut.

For diffractive optics, zone step height is a crucial factor for deciding the performance and efficiency of the whole optical element. For measurement of the zone step height of diffractive rings surface finish over zones (Sa, Ra), a

non-contact type CCI optical profiler is used. The respective 3D measurements of zone step height are shown in Fig. 11 (b), which are taken using a 20X objective with a scan area of 0.8mm x 0.8mm. The step height is found 1.276µm with an error of 0.113 µm. Fig. 11 (b) shows the surface roughness (Sa) profile of the aspheric diffractive surface where the Sa value is around 4.5 nm in the first experimental trial.

This step height value of the fabricated component is further used to calculate the efficiency of the aspheric diffractive component. Eq. 1.1 is adopted to calculate the efficiency of the diffractive optical element with the achieved value of step height d_0 achieved after machining. Here efficiency is 97.5% (calculate from Eq. 1.1 and λ_0 =3.828825 µm). For optical applications, minimum profile error is desirable, so further compensation is done to reduce the profile error and improves step height.

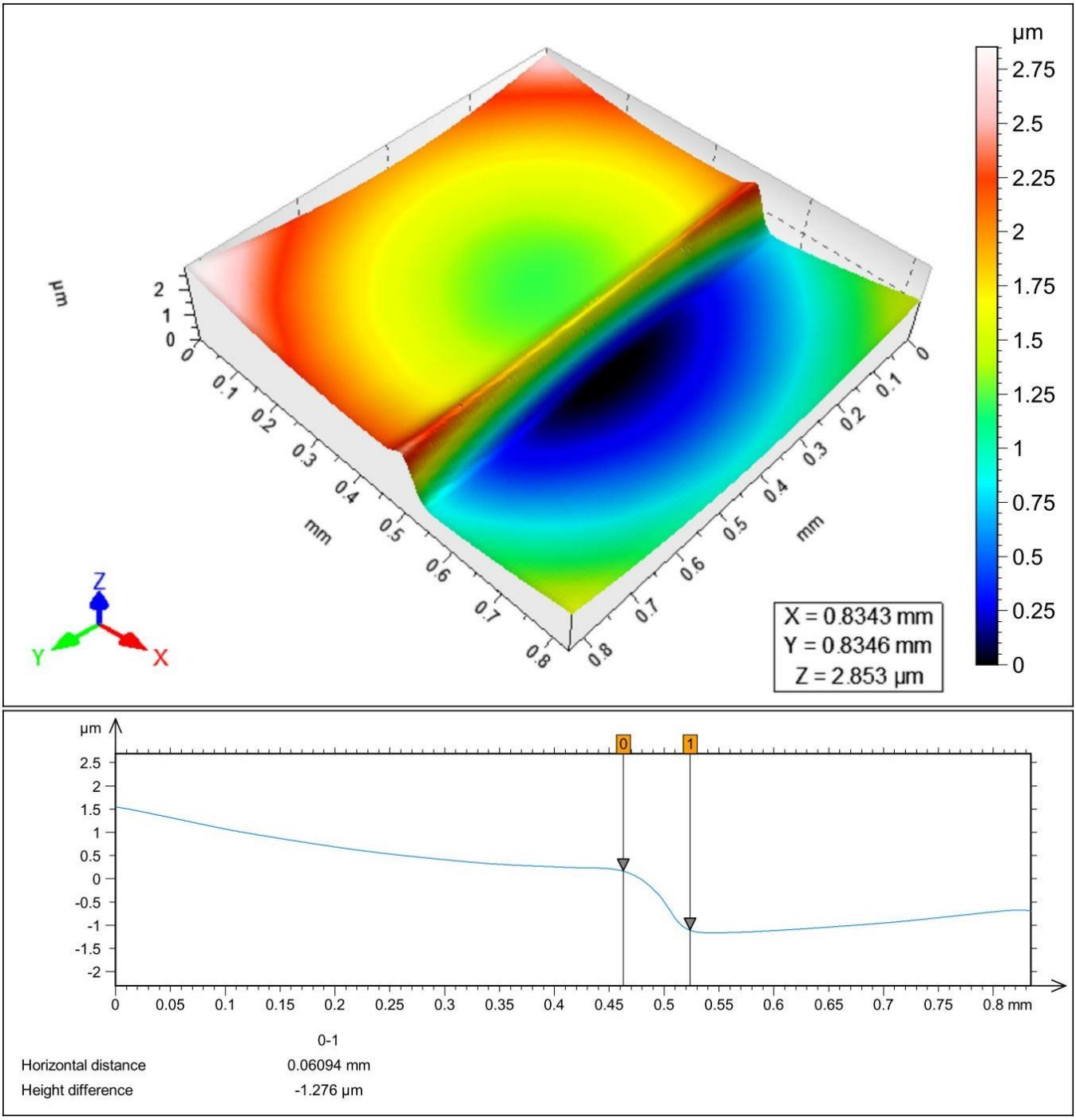

Fig. 11. (a) 3D plot for step height measurement.

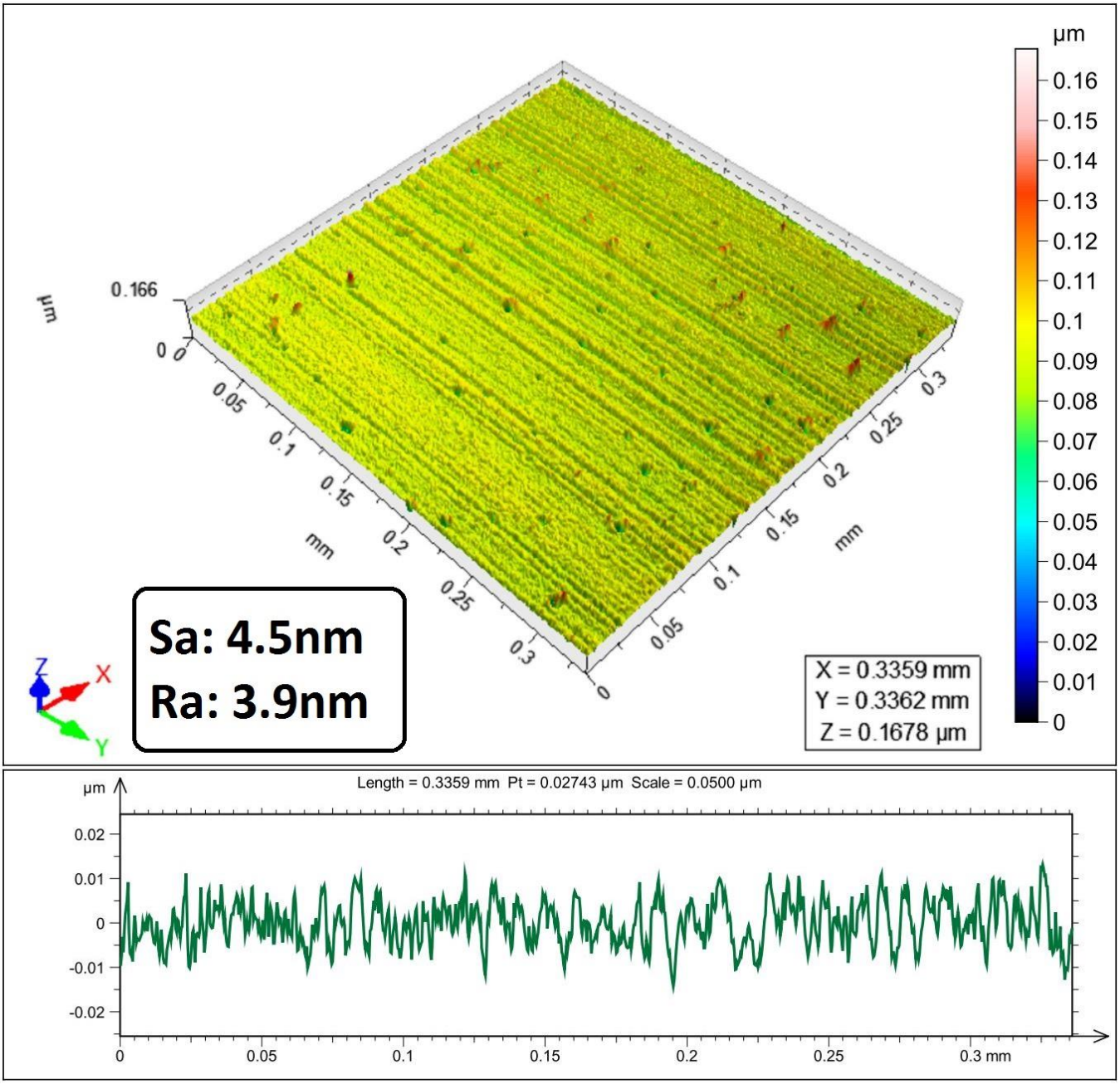

Fig. 11. (b) 3D Roughness plot.

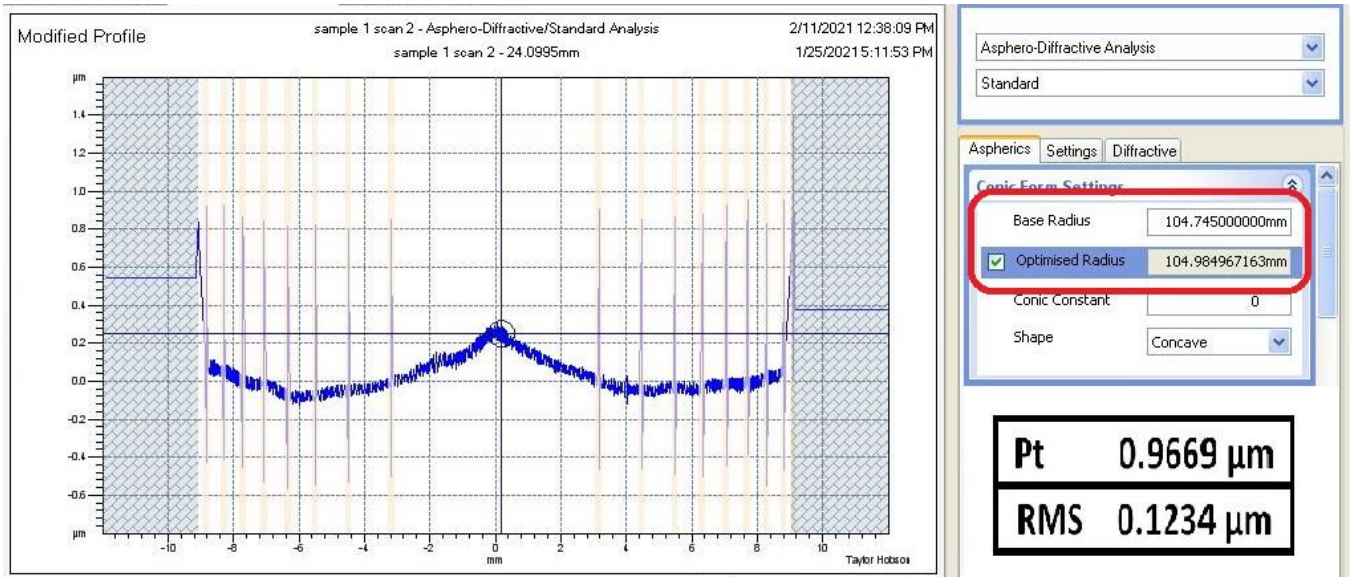

Fig. 11. (c) P_t curve obtained after analysing by aspheric utility software.

Over the past decades, many researchers have worked on tooth path compensation in diamond turning of lenses, structured surfaces and freeform optics. Tool path compensation is a well-known technique through which surface error can be reduced by modifying the tool motion. In this paper, one of the quite popular tool path compensation techniques proposed by Li et al. [38] is used. Li et al. proposed a novel compensation method for the diffractive-reflective hybrid objective lens (DHOL), through superimposing the hybrid surface with a small curvature to compensate for optical deviation there by improving the diffractive performance.

Once the tool path and machining conditions are fixed, the surface deviations are caused due to machining dynamics. These dynamics associated with residual errors, such as form error and figure errors. The measured data points are then analysed for the parameter of interest, i.e., form error, waviness, and step height. As discussed earlier, the error is quantified by comparing the machined surface/features with the design surface using aspheric analysis utility software. The MOD (.mod) file generated from aspheric analysis utility software was further imported to Diffsys® software to compensate for the original tool path. The error data point profile is firstly mirrored and then superimposed onto the original tool path to generate a modified tool path. Fig.12 illustrates the tool path compensation cycle, where the modified tool path is used to generate the required surface. This compensation process is repeated till the desired surface quality is achieved.

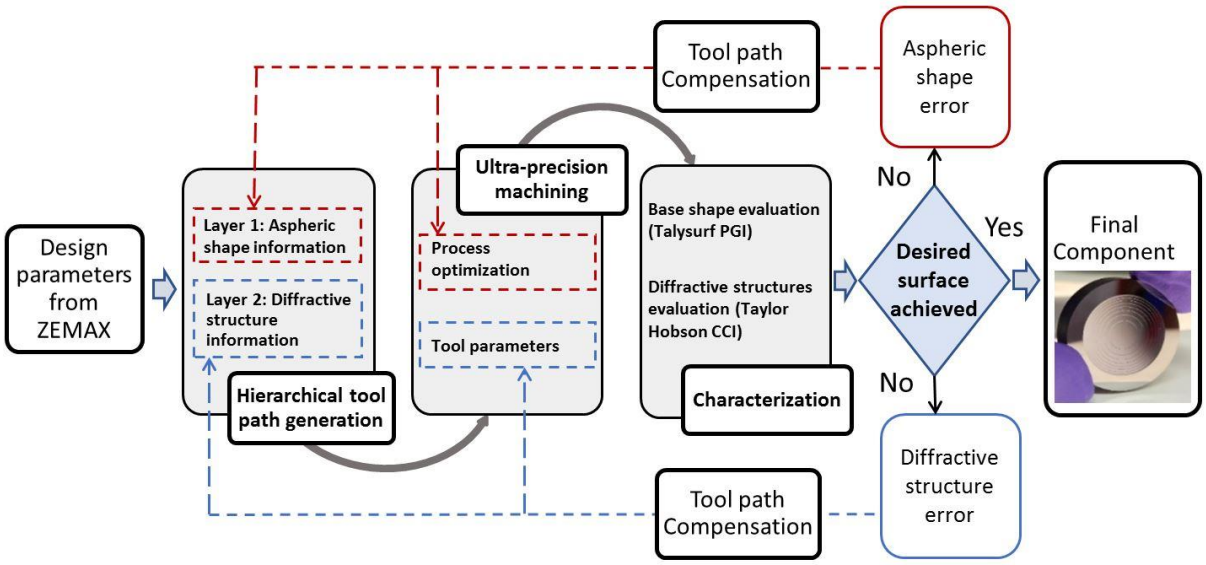

Fig. 12. Compensation cycle used in this study.

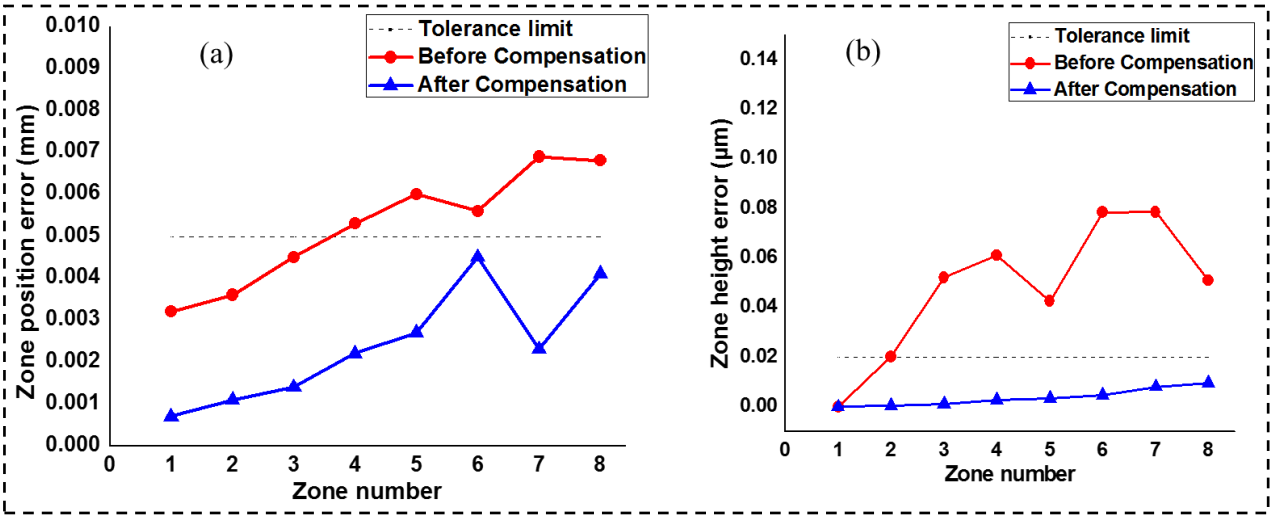

Fig. 13. Improvement in (a) Zone position accuracy and (b) Step height after compensation.

Again, fabrication is performed (trial 2) with compensated tool path maintaining all the other tool and machine parameters the same as in trial 1. After trial 2, the same metrology path is followed as in the case of trial 1. Fig. 14 (c) shows the surface plot depicting the radius of curvature value of 104.744 mm while the designed value was 104.745 mm. The error in radius is 0.001 mm, which is acceptable in case of profile error. The profile error of 0.2513 µm is obtained after compensation. A detailed comparison of step height and position accuracy is made to demonstrate the improvement through tool path compensation. Fig. 13 (a) shows the significant improvement in zone position accuracy after compensation; the position accuracy of all the zones is better than 5µm. Similarly, the step height of each zone is verified to know the improvement after compensation. The accuracy of all the steps is found to be better than 10 nm.

Step height is evaluated using CCI after implementing compensation. Fig. 14 (a) is shown to demonstrate the step height after compensation. i.e 1.387 µm with 0.8mm x 0.8mm scan area. The designed value is 1.388 µm, and the fabricated height is 1.387 µm; hence the error is only 0.001 µm. Fig. 13 (b) shows the improvement in step height at each zone. The step height error is reduced significantly, and each zone is fabricated with a step height error of less than 10 nm.

This step height (1.387 µm) is further used to calculate the diffractive efficiency of the component, where efficiency of around 99.57% is achieved, which is greater than the previous value (η=97.5%). Fig. 14 (b) shows the 3D surface roughness plot of the aspheric diffractive profile achieving surface roughness (Sa) of 3.5 nm after compensation. As compared to the first trial, the Ge aspheric diffractive lens obtained after compensation as shown in Fig.15 has better uniformity and surface finish.

5. Conclusion

The germanium aspheric diffractive surface can substantially benefit to many IR optical systems. SPDT is the most effective and mature method for producing accurate aspheric diffractive surfaces. The precise machine control, the selection of suitable diamond tools and the optimum choice of critical machining parameters are the most important aspects of this fabrication technology for achieving better surface finish, profile accuracies, and high diffraction efficiency. Some of the significant findings are listed below:

- An aspheric diffractive lens on germanium is designed and fabricated. Further, Metrology of the asphero diffractive lens is demonstrated with optical profilometry.
- The measured surface is compared with the designed surface to calculate the profile and step height error.
- The surface roughness of germanium aspheric diffractive optical element is achieved at 3.5 nm.
- The step height of diffractive grooves is achieved at 1.387µm with an error of 1 nm.
- The radial error of 0.001 mm and profile error of 0.2513 µm is achieved.
- The Diffractive efficiency is also calculated using the step height of the diffractive grooves. The maximum theoretical diffractive efficiency is achieved at 99.57% for 1.387µm step height.

Overall, this work has opened up new possibilities for fabricating complex hybrid profiles on useful brittle materials by selecting optimum machining parameters, tool parameters and precision machine control to increase the overall efficiency of the optical systems.

Funding

Not applicable.

Declaration of Competing Interest

The authors report that they have no competing interests.

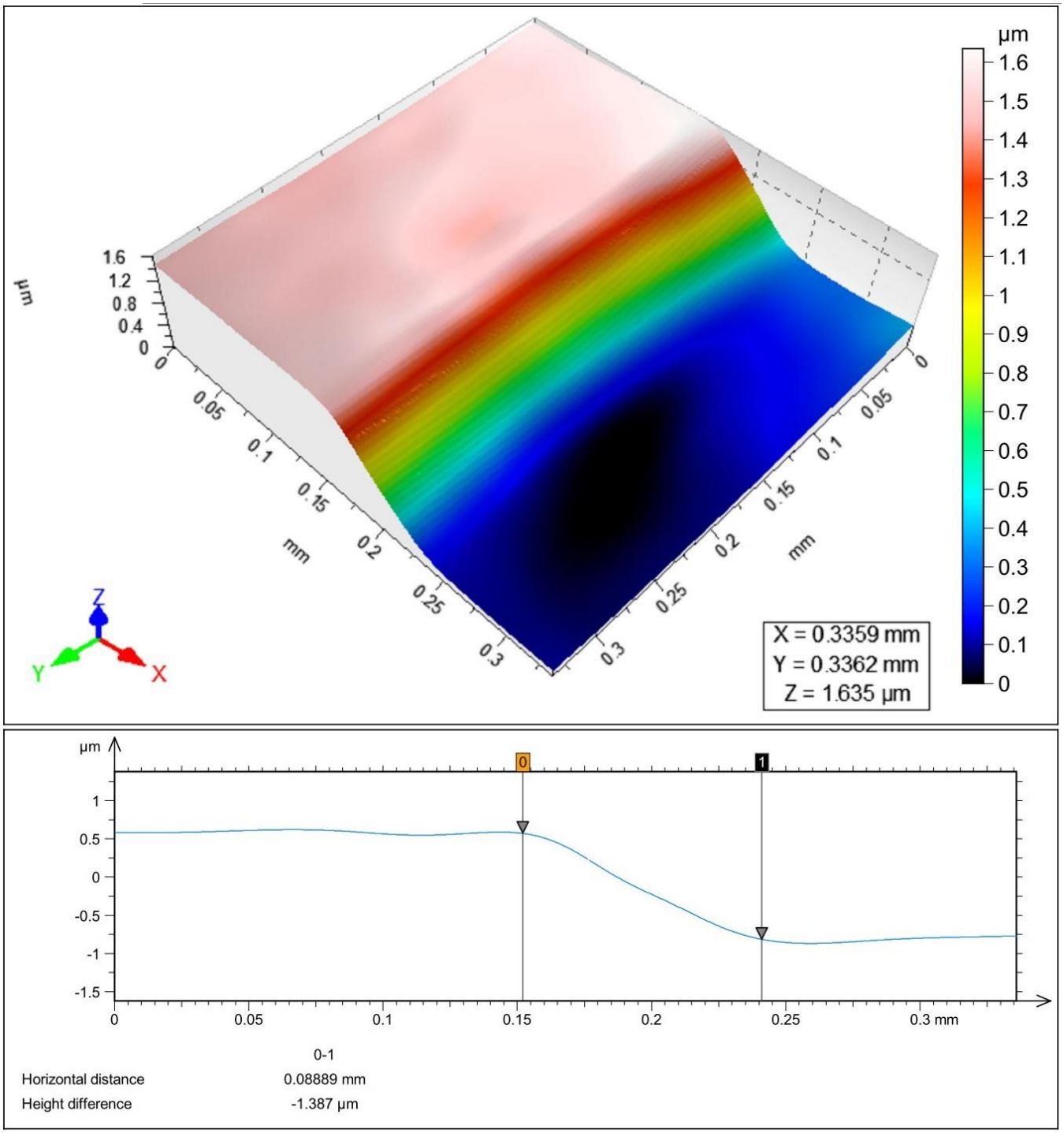

Fig. 14. (a) 3D plot for step height measurement.

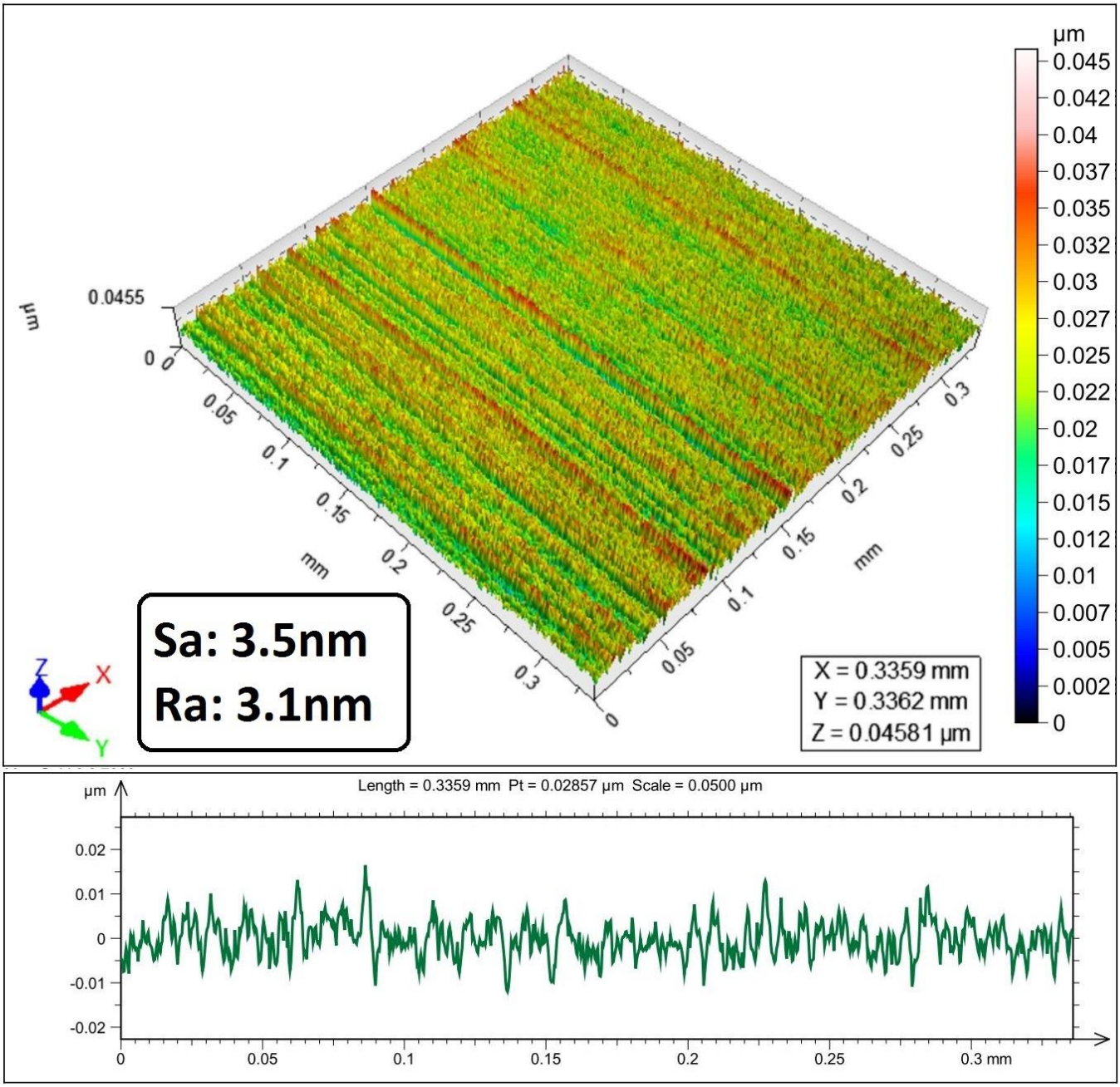

Fig. 14. (b) 3D Roughness plot.

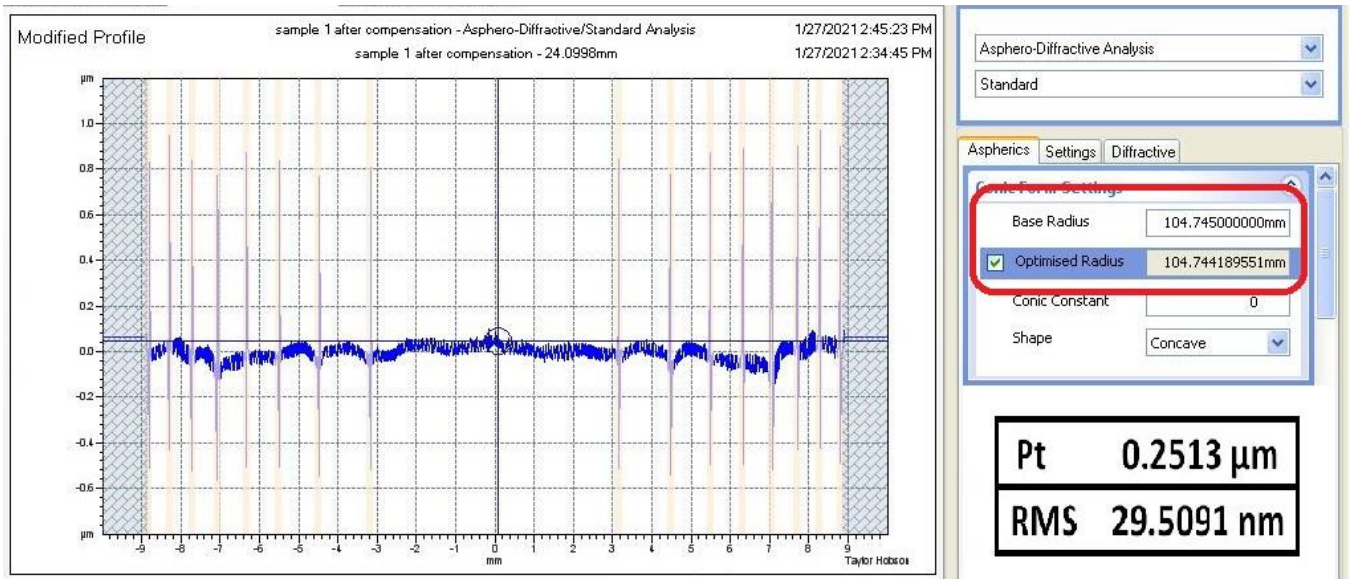

Fig. 14. (c) P_t curve obtained after analysing by aspheric utility software.

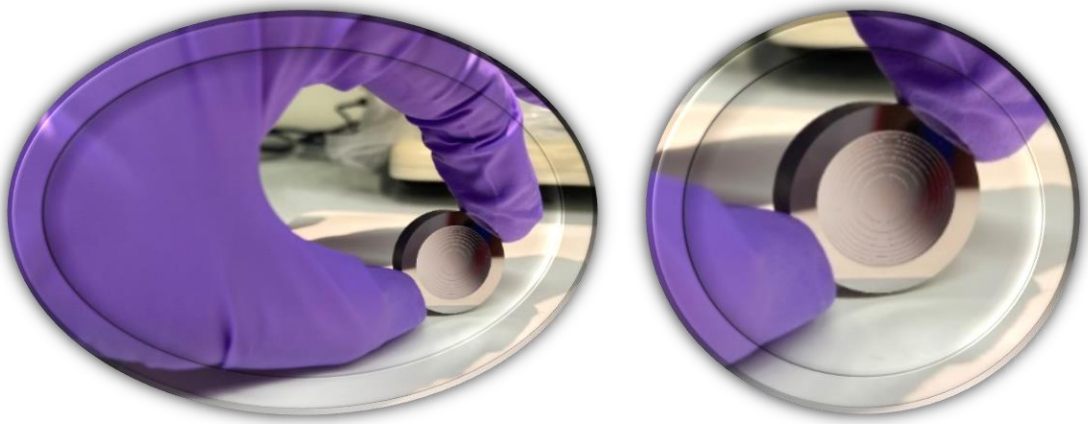

Fig. 15. Germanium aspheric diffractive optical element fabricated.

References

[1] A. Bruzzone, H. Costa, P. Lonardo, D. Lucca, Advances in engineered surfaces for functional performance, CIRP annals, 57 (2008) 750-769, https://doi.org/10.1016/j.cirp.2008.09.003.
[2] S. Kim, S. Chang, S. Pak, K.J. Lee, B. Jeong, G.-j. Lee, G.H. Kim, S.K. Shin, S.M. Yoo, Fabrication of electroless nickel plated aluminum freeform mirror for an infrared off-axis telescope, Applied optics, 54 (2015) 10137-10144, https://doi.org/10.1364/AO.54.010137.
[3] M. Alshami, A. Wabby, M. Mousselly, Design and development of Binary Diffractive Germanium Lens by thin film deposition, Journal of the European Optical Society-Rapid publications, 10 (2015), https://doi.org/10.2971/jeos.2015.15055.
[4] Y. Xie, Z. Lu, F. Li, J. Zhao, Z. Weng, Lithographic fabrication of large diffractive optical elements on a concave lens surface, Optics Express, 10 (2002) 1043-1047, http://doi.org/10.1364/OE.18.025102.
[5] G. Curatu, Design and fabrication of low-cost thermal imaging optics using precision chalcogenide glass molding, in: Current Developments in Lens Design and Optical Engineering IX, International Society for Optics and Photonics, 2008, pp. 706008.
[6] R. Kasztelanic, I. Kujawa, R. Stępień, R. Buczyński, Fabrication and application of soft glass micro-optical elements for midIR fiber optics, in: 2014 Third Mediterranean Photonics Conference, IEEE, 2014, pp. 1-3.
[7] H.-J. Kim, Y. Hwang, J.C. Jeong, J.-H. Kim, Fabrication of molded chalcogenide-glass lens for thermal imaging applications, Applied optics, 51 (2012) 5649-5656, https://doi.org/10.1364/AO.51.005649.
[8] E. Brinksmeier, O. Riemer, R. Gläbe, B. Lünemann, C. Kopylow, C. Dankwart, A. Meier, Submicron functional surfaces generated by diamond machining, CIRP annals, 59 (2010) 535-538, https://doi.org/10.1016/j.cirp.2010.03.037.
[9] Y. Fu, N.K.A. Bryan, Influence of astigmatism on the fabrication of diffractive structures by use of focused ion-beam milling, Optics Express, 12 (2004) 3954-3966, https://doi.org/10.1364/OPEX.12.003954.
[10] K. Haskic, S. Kühne, B. Löchel, M. Schmidt, 3D nanometer features by ultra precision machining, Microsystem technologies, 20 (2014) 2051-2053, https://doi.org/10.1007/s00542-013-2059-6.
[11] S. Kühne, K. Haskic, S. Lemke, M. Schmidt, Fabrication and characterization of machined 3D diffractive optical elements, Microsystem technologies, 20 (2014) 2103-2107, https://doi.org/10.1007/s00542-014-2122-y.
[12] Z. Xu, F. Fang, S. Zhang, X. Zhang, X. Hu, Y. Fu, L. Li, Fabrication of micro DOE using micro tools shaped with focused ion beam, Optics Express, 18 (2010) 8025-8032, https://doi.org/10.1364/OE.18.008025.
[13] J. Yan, K. Maekawa, J.i. Tamaki, A. Kubo, Experimental study on the ultraprecision ductile machinability of single-crystal germanium, JSME International Journal Series C Mechanical Systems, Machine Elements and Manufacturing, 47 (2004) 29-36, https://doi.org/10.1299/jsmec.47.29.
[14] L. Li, Y.Y. Allen, C. Huang, D.A. Grewell, A. Benatar, Y. Chen, Fabrication of diffractive optics by use of slow tool servo diamond turning process, Optical Engineering, 45 (2006) 113401, http://doi.org/ 10.1117/1.2387142.
[15] A. Meier, Diamond turning of diffractive microstructures, Precision Engineering, 42 (2015) 253-260, https://doi.org/10.1016/j.precisioneng.2015.05.007.
[16] M. Rayer, D. Mansfield, Chromatic confocal microscopy using staircase diffractive surface, Applied optics, 53 (2014) 5123-5130, https://doi.org/10.1364/AO.53.005123.
[17] K. Fuse, T. Okada, K. Ebata, Diffractive/refractive hybrid F-theta lens for laser drilling of multilayer printed circuit boards, in: International Congress on Applications of Lasers & Electro-Optics, Laser Institute of America, 2001, pp. 1666-1675, https://doi.org/10.2351/1.5059839.
[18] Y. Su, X. Chen, X. Guo, G. Rui, X. Liu, F. Zhang, C. Yang, Y. Xiao, Z. Xu, New fabrication technology in single point diamond turning for IR aspheric optical parts, in: 7th International Symposium on Advanced Optical Manufacturing and Testing Technologies: Advanced Optical Manufacturing Technologies, International Society for Optics and Photonics, 2014, pp. 92811L, https://doi.org/10.1117/12.2069649.

[19] J. Yan, K. Maekawa, J.i. Tamaki, T. Kuriyagawa, Micro grooving on single-crystal germanium for infrared Fresnel lenses, Journal of micromechanics and microengineering, 15 (2005) 1925, http://doi.org/10.1088/0960-1317/15/10/019.
[20] P.N. Blake, R.O. Scattergood, Ductile-regime machining of germanium and silicon, Journal of the American ceramic society, 73 (1990) 949-957, https://doi.org/10.1111/j.1151-2916.1990.tb05142.x.
[21] R.G. Jasinevicius, J.G. Duduch, A.J. Porto, Investigation on diamond turning of silicon crystal-generation mechanism of surface cut with worn tool, Journal of the Brazilian Society of Mechanical Sciences, 23 (2001) 241-252, https://doi.org/10.1590/S0100-73862001000200010.
[22] T. Ohta, J. Yan, S. Yajima, Y. Takahashi, N. Horikawa, T. Kuriyagawa, High-efficiency machining of single-crystal germanium using large-radius diamond tools, International Journal of Surface Science and Engineering, 1 (2007) 374-392, https://doi.org/10.1504/IJSURFSE.2007.016691.
[23] R.G. Jasinevicius, J.G. Duduch, G.A. Cirino, P.S. Pizani, Diamond turning of small Fresnel lens array in single crystal InSb, Journal of micromechanics and microengineering, 23 (2013) 055025, http://doi.org/10.1088/0960-1317/23/5/055025.
[24] R.G. Jasinevicius, J.G. Duduch, P.S. Pizani, Structure evaluation of submicrometre silicon chips removed by diamond turning, Semiconductor science and technology, 22 (2007) 561, https://doi.org/10.1088/0268-1242/22/5/019.
[25] Y. Zhang, Z. Wang, F. Zhang, H. Qin, J. Li, Y. Mai, Processing and error compensation of diffractive optical element, in: 7th International Symposium on Advanced Optical Manufacturing and Testing Technologies: Large Mirrors and Telescopes, International Society for Optics and Photonics, 2014, pp. 92800G, http://doi.org/10.1117/12.2068106.
[26] P. Wang, N. Mohammad, R. Menon, Chromatic-aberration-corrected diffractive lenses for ultra-broadband focusing, Scientific reports, 6 (2016) 1-7, https://doi.org/10.1038/srep21545.
[27] G.I. Greisukh, I.y.A. Levin, E.G. Ezhov, Design of Ultra-High-Aperture Dual-Range Athermal Infrared Objectives, in: Photonics, MDPI, 2022, pp. 742. https:// doi.org/10.3390/photonics9100742
[28] H. Yang, C. Xue, C. Li, J. Wang, Optimal design of multilayer diffractive optical elements with effective area method, Applied Optics, 55 (2016) 1675-1682.
[29] V. Laborde, J. Loicq, J. Hastanin, S. Habraken, Multilayer diffractive optical element material selection method basedon transmission, total internal reflection, and thickness, Applied Optics, 61 (2022) 7415-7423. https://doi.org/10.1364/AO.465999
[30] S. Berwal, N. Khatri, D. Kim, A review on design modalities of solar-pumped solid-state laser, Applied Surface Science Advances, 12 (2022) 100348, https://doi.org/10.1016/j.apsadv.2022.100348.
[31] K. Manjunath, S. Tewary, N. Khatri, K. Cheng, Monitoring and Predicting the Surface Generation and Surface Roughness in Ultraprecision Machining: A Critical Review, Machines, 9 (2021) 369, https://doi.org/10.3390/machines9120369.
[32] R. Bittner, Tolerancing of single point diamond turned diffractive optical elements and optical surfaces, Journal of the European Optical Society-Rapid Publications, 2 (2007).
[33] X. Gao, C. Xue, Y. Chao, Y. Liu, Optimization method of manufacturing for diamond turning soft-brittle materials' harmonic diffractive optical elements, Applied Optics, 60 (2021) 162-171. https://doi.org/10.1364/AO.411706.
[34] R. Sharma, V. Mishra, H. Garg, N. Khatri, R.V. Sarepaka, V. Karar, Effect of machining parameters on surface finish and subsurface damage for diamond-turned germanium, Journal of the Brazilian Society of Mechanical Sciences and Engineering, 42 (2020) 1-10. https://doi.org/10.1007/s40430-020-2240-7
[35] S. Gupta, N. Khatri, V. Mishra, V. Karar, S. Dhami, Optimization of process parameters for fabrication of IR aspheric diffractive based on the response surface methodology, in: International Conference on Fibre Optics and Photonics, Optica Publishing Group, 2016, pp. Th3A. 5.
[36] S. Gupta, N. Khatri, V. Karar, S. Dhami, Investigation of Surface Roughness of Single Point Diamond Turned Germanium Substrate by Coherence Correlation Interferometry and Image Processing, in: IOP Conference Series: Materials Science and Engineering, IOP Publishing, 2016, pp. 012032. http://iopscience.iop.org/1757-899X/149/1/012032.
[37] S.P. Yadav, H. Shaikh, R.S. Pawade, Assessment of optical performance of aspheric germanium lens manufactured using single point diamond turning, in: International Manufacturing Science and

Engineering Conference, American Society of Mechanical Engineers, 2017, pp. V001T002A010. http://doi.org/10.1115/MSEC2017-2691
[38] L. Li, C. Chan, W. Lee, Y. Liu, A novel evaluation and compensation method for ultra-precision machining of hybrid lens, Precision Engineering, 43 (2016) 10-23. https://doi.org/10.1016/j.precisioneng.2015.05.001.